McMahon, B. T. *et al.* (2013). *Géotechnique* **63**, No. 9, 746–752 [http://dx.doi.org/10.1680/geot.12.P.061]

Cavity expansion model for the bearing capacity and settlement of circular shallow foundations on clay

B. T. McMAHON*, S. K. HAIGH* and M. D. BOLTON*

The use of an ellipsoidal cavity expansion model to estimate the bearing capacity and settlement of circular shallow foundations on clay is presented. The model uses an upper-bound energy approach with contours of constant soil displacement taken to be ellipsoidal within a hemispherical outer boundary. The elastic and plastic work done within the soil are equated to the footing work, with yield being defined using the von Mises' yield criterion. It is shown that, for two different soil rigidities, results are consistent with those obtained from finite-element analyses available in the literature. A relationship between the bearing stress on a circular shallow foundation and its normalised settlement is developed, with an expression provided for the linear working range.

KEYWORDS: bearing capacity; clays; plasticity; settlement

INTRODUCTION

The design of a shallow foundation requires consideration of the ultimate bearing capacity, and of the settlement at the working load. Settlements are often critical, owing to the vulnerability of typical structures to differential settlements.

There are two approaches that can be adopted in determining the bearing capacity of foundations. For shallow foundations, a local mechanism of indentation, shear and heaving is invoked, which leads to Terzaghi's bearing capacity equation (Terzaghi, 1943). For the particular case of a shallow foundation on the surface of a purely cohesive soil with undrained shear strength c_u, the bearing capacity, q_{ult}, is determined using

$$q_{ult} = c_u N_c s_c \quad (1)$$

where N_c and s_c are the bearing capacity and shape factors respectively. Prandtl (1921) used plasticity theory to determine for a strip footing on the surface that $N_c = 2 + \pi = 5{\cdot}14$. Refinements have been made to the equation since, including research on different-shaped footings and the effects of embedment, footing roughness and soil profile. Cox *et al.* (1961) determined that $N_c = 5{\cdot}69$ for a smooth circular footing, and Eason & Shield (1960) found that $N_c = 6{\cdot}05$ for a rough circular footing. The program Analysis of Bearing Capacity (ABC) (Martin, 2003) supports these values, with an example of the characteristic net being shown in Fig. 1(a).

Concerns about the use of a rigid-plastic material to represent soil led to the second approach for determining foundation stiffness and ultimate bearing capacity: a cavity expansion idealisation. This method has been used primarily for deep foundations such as piles, where capacity is provided by the resistance that the soil offers to the expansion of a cavity corresponding to the volume indented by the pile. Using spherical cavity expansion theory combined with plasticity, the bearing capacity factor has been determined to be a function of both the strength and the stiffness of the soil. This arises from the recognition that soil in the far field must remain elastic if the indentation of the foundation

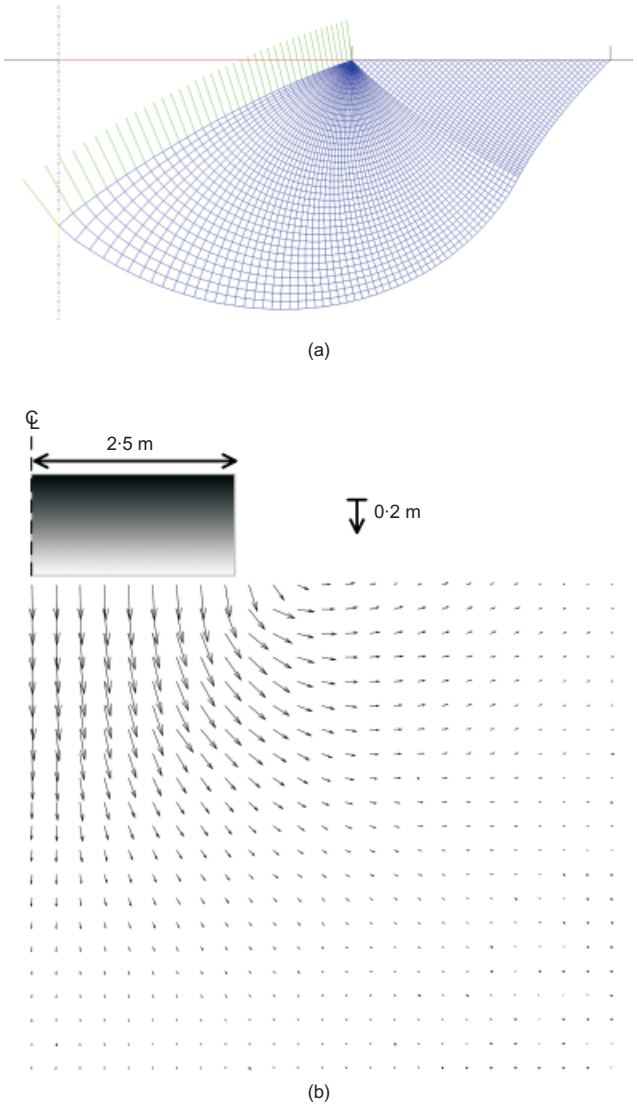

Fig. 1. Mechanisms beneath shallow foundations: (a) stress characteristic method from ABC (Martin, 2003) for Prandtl mechanism; (b) undrained mechanism at prototype scale from centrifuge testing

Manuscript received 3 May 2012; revised manuscript accepted 12 October 2012. Published online ahead of print 31 January 2013. Discussion on this paper closes on 1 December 2013, for further details see p. ii.

* Department of Engineering, University of Cambridge, UK.

remains finite. Bishop *et al.* (1945) investigated the theory of indentation, and determined the pressure required to enlarge a spherical cavity infinitely through plastic flow, p_s, as

$$p_s = \frac{2Y}{3}\left(1 + 3\ln\frac{r_p}{r_c}\right) \tag{2}$$

where Y is the uniaxial yield stress of the material and

$$\frac{r_p}{r_c} = \left[\frac{E}{(1+\nu)Y}\right]^{1/3} \tag{3}$$

Assuming that for soil Y is equivalent to the triaxial deviatoric stress q_u, and assuming undrained behaviour, for which $\nu = 0{\cdot}5$ and $E = 3G$, this predicts the limiting stress for expansion of a spherical cavity as

$$p_s = \frac{2}{3}q_u\left[1 + \ln\left(2\frac{G}{q_u}\right)\right] \tag{4}$$

Finite-element analyses have been widely used in the consideration of the bearing capacity of shallow foundations. Taiebat & Carter (2000) performed an analysis producing $N_c = 5{\cdot}7$ for a rough footing on clay with $G/c_u = 100$. This was refined by Taiebat & Carter (2010), through use of a finer mesh and selection of a flow rule closer to the Tresca criterion, to produce a more accurate value of $N_c = 6{\cdot}17$ for the same soil. Gourvenec & Randolph (2002) investigated stiffer clay, with $G/c_u = 167$, determining the ultimate bearing capacity factor to be $N_c = 5{\cdot}91$. These values are respectively 5·8% less, 2·0% more and 2·4% less than the classical value of $N_c = 6{\cdot}05$.

Centrifuge tests of shallow circular foundations, lowered at 100***g*** onto the surface of kaolin clay, have been performed in Cambridge (McMahon, 2012). The immediate undrained displacement field measured in a typical test using particle image velocimetry (White *et al.*, 2003) is shown in Fig. 1(b). It can be seen that the displacement field more closely resembles a cavity expansion than a Prandtl-style mechanism such as that shown in Fig. 1(a).

This paper demonstrates a method for determining the load–settlement behaviour of a circular surface foundation on linear-elastic perfectly plastic soil using an energy approach based on a kinematically admissible deformation mechanism for cavity expansion. In order to evolve smoothly from a plane punch at the foundation to a hemispherical cavity expansion at depth, the cavity expansion is taken to be ellipsoidal rather than spherical, as an approximation to the behaviour seen in the centrifuge test data.

ANALYSIS PROCEDURE

In order to carry out an analysis based on energy conservation, it is necessary to calculate the work done in deforming the soil within the axisymmetric mechanism. Rigid, perfectly plastic analyses in plane strain can calculate the work done per unit volume, following Shield & Drucker (1953), as

$$W = c_u\varepsilon_1 \tag{5}$$

However, for an elastic perfectly plastic material in axial symmetry, it is important to calculate both the elastic and the plastic work due to all of the stress components acting on the soil.

Elastic work

The energy associated with elastic work can be determined using Hooke's law. For the undrained case with Poisson's ratio $\nu = 0{\cdot}5$, the three-dimensional expression can be reduced to

$$E\begin{bmatrix}\varepsilon_1\\ \varepsilon_2\end{bmatrix} = \begin{bmatrix}1 & -\frac{1}{2}\\ -\frac{1}{2} & 1\end{bmatrix}\begin{bmatrix}\sigma_1 - \sigma_3\\ \sigma_2 - \sigma_3\end{bmatrix} \tag{6}$$

As the undrained Young's modulus, E_u, is related to the shear modulus, G, by $E_u = 3G$, this can be inverted to give

$$\begin{bmatrix}\sigma_1 - \sigma_3\\ \sigma_2 - \sigma_3\end{bmatrix} = G\begin{bmatrix}4 & 2\\ 2 & 4\end{bmatrix}\begin{bmatrix}\varepsilon_1\\ \varepsilon_2\end{bmatrix} \tag{7}$$

The rate of elastic work per unit volume is given by

$$\frac{\partial W_e}{\partial \delta_f} = \sigma_1\dot{\varepsilon}_1 + \sigma_2\dot{\varepsilon}_2 + \sigma_3\dot{\varepsilon}_3 \tag{8}$$

If a mechanism that is geometrically similar for all foundation displacements is assumed, then it can be shown that

$$\varepsilon_n = \frac{\partial \varepsilon_n}{\partial \delta_f}\delta_f = \dot{\varepsilon}_n\delta_f \quad n = 1,\ 2,\ 3 \tag{9}$$

Given that there is no volumetric strain, $\varepsilon_3 = -\varepsilon_1 - \varepsilon_2$, and thus equations (7) and (8) give the elastic work rate per unit volume

$$\frac{\partial W_e}{\partial \delta_f} = 4G\hat{\dot{\varepsilon}}^2\delta_f \tag{10}$$

where the strain invariant is given by

$$\hat{\dot{\varepsilon}}^2 = \left[\dot{\varepsilon}_1^2 + \dot{\varepsilon}_2^2 + \dot{\varepsilon}_1\dot{\varepsilon}_2\right] \tag{11}$$

Plastic work

Yield was determined using the isotropic von Mises' yield criterion

$$(\sigma_1 - \sigma_3)^2 + (\sigma_2 - \sigma_3)^2 + (\sigma_1 - \sigma_2)^2 = 2q_u^2 \tag{12}$$

where q_u is the undrained strength in triaxial compression. Substitution of the expressions in equations (7) and (11) into equation (12) shows that, at yield

$$\hat{\dot{\varepsilon}} = \frac{1}{2\sqrt{3}}\frac{q_u}{G}\frac{1}{\delta_f} \tag{13}$$

It can be shown from equation (6) that, for an undrained elastic material, the total strain vector is parallel to the deviatoric stress, $\hat{\sigma} = \sigma - p$. As the von Mises' yield criterion is circular in the π-plane, for a material exhibiting associated flow, the direction of the incremental plastic strain vector, $\dot{\varepsilon}_p$, is also parallel to the deviatoric stress. If a mechanism that remains geometrically similar for all footing displacements is assumed, the direction of the total strain vector will remain constant under both elastic and plastic deformations. As the plastic and total strain rates are parallel, it is thus implied that no further elastic strain can occur post-yield, with the plastic strain rate being equal to the total strain rate. It thus follows that, in the zone of plastic deformation, no incremental elastic work is done.

As the total strain rate in the plastic zone is equal to the plastic strain rate, it follows that

$$\frac{\hat{\sigma}_2}{\hat{\sigma}_1} = \frac{\dot{\varepsilon}_2}{\dot{\varepsilon}_1} \tag{14a}$$

and

$$\frac{\hat{\sigma}_3}{\hat{\sigma}_1} = \frac{\dot{\varepsilon}_3}{\dot{\varepsilon}_1} \tag{14b}$$

This can be substituted, along with the condition of no volumetric strain, into the yield criterion of equation (12). This produces an expression for the major principal deviatoric stress

$$\hat{\sigma}_1 = \frac{q_u \dot{\varepsilon}_1}{\sqrt{3}\hat{\dot{\varepsilon}}} \tag{15}$$

The rate of plastic work due to the deviatoric stress per unit volume is given by

$$\frac{\partial W_p}{\partial \delta_f} = \hat{\sigma}_1 \dot{\varepsilon}_1 + \hat{\sigma}_2 \dot{\varepsilon}_2 + \hat{\sigma}_3 \dot{\varepsilon}_3 \tag{16}$$

Substitution of the expressions in equations (14) and (15) determines the plastic work rate per unit volume to be

$$\frac{\partial W_p}{\partial \delta_f} = \frac{2 q_u \hat{\dot{\varepsilon}}}{\sqrt{3}} \tag{17}$$

The validity of the discussed approach is verified by analysing an elastic perfectly plastic spherical cavity expansion and comparing this with the results presented by Bishop *et al.* (1945).

VALIDATION OF MODEL

Using the energy method discussed, a solution can be determined for the expansion of a spherical cavity. Equations (8), (10), (11), (16) and (17) are utilised, but the derivatives are now taken with respect to cavity expansion, ρ, rather than footing displacement. The radial displacement of a spherical cavity is given as

$$\rho = \frac{dV}{4\pi r^2} \tag{18}$$

where dV is the change in cavity volume. The radial and circumferential strains, also the principal strains, are

$$\varepsilon_r = \frac{2\rho}{r} = \frac{dV}{2\pi r^3} \tag{19a}$$

$$\varepsilon_\theta = -\frac{\rho}{r} = -\frac{dV}{4\pi r^3} \tag{19b}$$

which can be substituted into equation (11) to find that

$$\hat{\dot{\varepsilon}} = \frac{\sqrt{3} r_c^2}{r^3} \tag{20}$$

This can now be compared with the value at yield given by equation (13) to show that

$$\begin{aligned} r_p^3 &= 6 r_c^2 \frac{G}{q_u} \rho \\ &= 2 r_c^3 \frac{dV}{V} \frac{G}{q_u} \end{aligned} \tag{21}$$

Equation (20) is utilised in calculating the rates of elastic and plastic work per unit volume as portrayed in equations (10) and (17) respectively. These work rates are then integrated over the volume to give a limiting stress of

$$\sigma_c = \frac{2}{3} q_u \left[1 + \ln\left(2 \frac{G}{q_u} \right) \right] \tag{22}$$

which is identical to the lower-bound solution of Bishop *et al.* (1945) shown in equation (4), which was based on equilibrium stresses that conform to the yield criterion.

The assumption of a deformation mechanism and the balancing of work and energy must, in principle, lead to an upper-bound estimate of collapse loads for perfectly rigid-plastic materials. Similarly, the assumption of an arbitrary but kinematically admissible deformation mechanism for elastic materials leads in principle to an overestimation of strain energy under an applied load, and to an underestimation of the displacement of its point of application. Accordingly, the energy method proposed here should provide an upper bound to the true load–displacement relationship (Klar & Osman, 2008). The equivalence of equations (22) and (4) simply confirms the exact nature of both the lower-bound and upper-bound solutions. In spherical symmetry, only one deformation mechanism is possible, so the upper and lower bounds naturally coincide at the correct solution. Equally, this confirms the accuracy of the upper-bound energy calculation.

CAVITY EXPANSION ANALYSIS OF CIRCULAR SHALLOW FOUNDATIONS

In this paper, an energy method is used to determine an upper bound on the bearing capacity of a circular shallow foundation using cavity expansion methods. Conventional cavity expansion methods assume expansion of a hemispherical cavity below the foundation, which expands outwards with spherical symmetry. These methods ignore the work done in the hemispherical zone below the foundation. In this paper an ellipsoidal cavity expansion approach is analysed, as this allows a smooth transition between a flat punch at the soil surface and spherical cavity expansion in the far field, allowing an upper-bound solution to be attempted.

Figure 2 illustrates notation and the global mechanism. In the near field, ellipsoids transition smoothly from a flat punch at the ground surface to a hemisphere of radius r_h. Beyond this radius, conventional spherical cavity expansion occurs. The plastic radius, r_p, divides the plastic and elastic zones of the soil, and can lie in either the ellipsoidal or the spherical zone. In order to make the calculation domain finite, a bounding radius, r_b, in the spherical zone is chosen, with the work done outside this radius being calculated on the basis of purely elastic spherical cavity expansion. This approach is valid provided $r_p < r_b$ for the foundation settlement considered.

An upper bound on the bearing capacity of a shallow foundation can be found by equating the work done in moving the foundation to the energy stored or dissipated within the soil using an assumed mechanism. In the case of the mechanism described here, this work can be subdivided into elastic work beyond the bounding radius and both elastic and plastic work within the bounding radius.

ASSUMED DEFORMATION FIELD

Ellipsoidal model

A new method is now used to describe the movement within the hemisphere of radius r_h in terms of a series of ellipsoids with a resultant soil displacement normal to the ellipsoid at each point. The first ellipsoid occurs at the footing base, and hence is the special case of a circle (the footing) with normal displacement δ_f. This corresponds to a perfectly rough footing base. Ellipsoids then grow in size and gradually transition towards being a hemisphere at r_h. Fig. 3 portrays the ellipsoids tending towards hemispheres at the hemispherical radius – in this case one footing diameter. The transition is accomplished through moving the foci of the ellipsoids, allowing their eccentricity to change. Compatibility is maintained using

$$w = \frac{A_f}{A_e} \delta_f \tag{23}$$

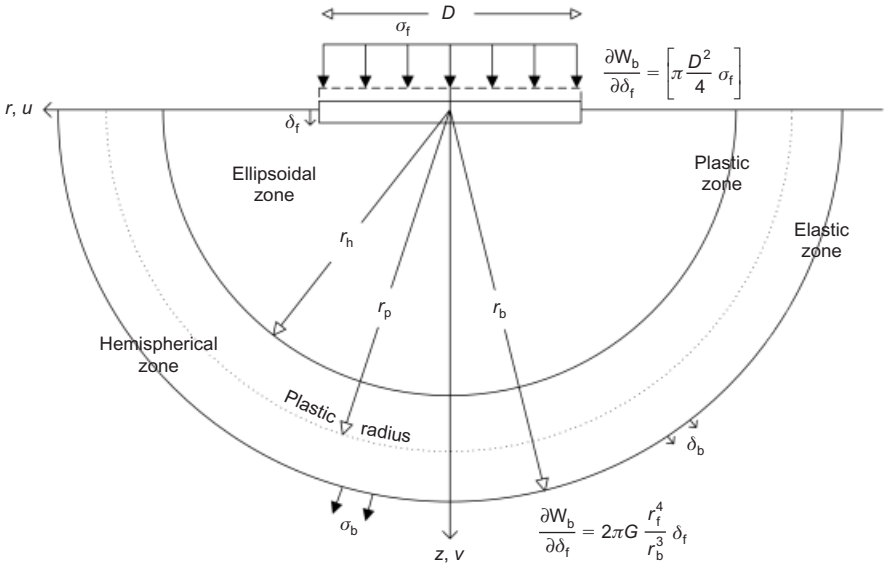

Fig. 2. Energy method used to determine load–settlement behaviour

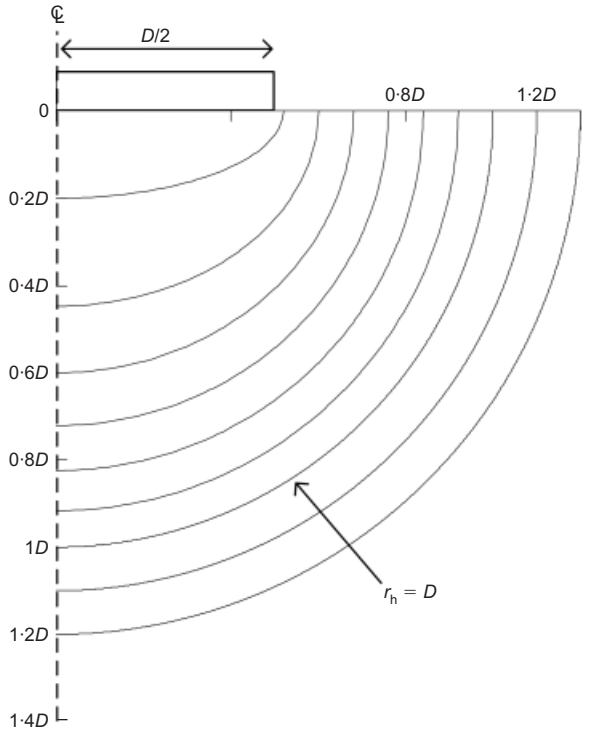

Fig. 3. Evolution of ellipsoids to hemispheres for $r_h = D$

where w is the displacement normal to the ellipsoid, and A_e and A_f are the surface areas of that ellipsoid and the footing respectively.

The axisymmetric nature of the problem results in the ellipsoids being oblate spheroids. The general equation of an oblate spheroid in cylindrical coordinates is given by

$$\frac{r^2}{a^2} + \frac{z^2}{b^2} = 1 \tag{24}$$

where $a > b$.

The focal radius of an ellipse can be expressed as

$$f = \sqrt{a^2 - b^2} \tag{25}$$

At the soil surface the ellipse is a straight line: thus $f = a = r_f$, $b = 0$, corresponding to a focus at the footing edge. Circles are a special case of an ellipse where $a = b$, corresponding to a focus at the centre. The analysis presented here allows the focal radius to vary from r_f to zero as a linear function of the major-axis radius a. The expression for the focal radius is thus given by

$$\begin{aligned} f &= \left(\frac{r_f}{r_f - r_h}\right) a - \frac{r_f r_h}{r_f - r_h} \\ &= \frac{r_f (a - r_h)}{r_f - r_h} \end{aligned} \tag{26}$$

The defined focus relationship in equation (26) can be used to produce an expression for the minor-axis radius, b, as

$$b^2 = a^2 - \frac{r_f^2 (a - r_h)^2}{(r_f - r_h)^2} \tag{27}$$

Substituting equation (27) into the general ellipse expression (equation (24)) produces a quartic equation in terms of the major axis radius a

$$\begin{aligned} &\left(r_h^2 - 2 r_f r_h\right) a^4 + \left(2 r_f^2 r_h\right) a^3 \\ &\quad + \left(2 r^2 r_f r_h - z^2 r_f^2 + 2 z^2 r_f r_h - z^2 r_h^2 - r^2 r_h^2 - r_f^2 r_h^2\right) a^2 \\ &\quad + \left(-2 r^2 r_f^2 r_h\right) a + r^2 r_f^2 r_h^2 = 0 \end{aligned} \tag{28}$$

A grid of points (r, z) was created and utilised in solving equation (28) using the *roots* function within Matlab. The major-axis radius, a, was thus determined for each point in the soil. The minor-axis radius, b, was then found using equation (27). The surface area of the ellipsoid, A_e, passing through each grid point could hence be calculated and consequently the magnitude of displacement at each point found.

The soil displacement is defined as being normal to the surface of the ellipsoid. The magnitude of displacement at each point is determined from equation (23), in which the surface area of half an oblate spheroid is given by

$$A_e = \pi a^2 + \frac{\pi a b^2}{2 f} \ln\left(\frac{a + f}{a - f}\right) \tag{29}$$

For ease of strain calculation, the displacement, w, was separated into radial and vertical components u and v, as shown in Fig. 2. The slope of the displacement vector, denoted $\mathrm{d}z/\mathrm{d}r$, was combined with the known displacement magnitude to produce

$$\frac{\mathrm{d}z}{\mathrm{d}r} = \frac{a^2}{b^2}\left(\frac{z}{r}\right) \tag{30a}$$

$$u = \frac{w}{\sqrt{1 + (\mathrm{d}z/\mathrm{d}r)^2}} \tag{30b}$$

$$v = u\frac{\mathrm{d}z}{\mathrm{d}r} \tag{30c}$$

Hemispherical region

Beyond the designated hemispherical boundary, the soil displacements are normal to hemispheres. Hemispheres are a particular case of an ellipsoid where $a = b = r$, and thus a similar approach can be adopted.

The deformation mechanism produced using this model is shown in Fig. 4. It must be noted that the mechanism suffers continuity issues at the footing edge, owing to a gross change in geometry: below the foundation soil displacements are purely vertical, whereas at the soil surface they are purely horizontal. Investigation demonstrated that changing the geometry at the footing edge had negligible effect on the values of footing pressure and settlement.

The strains within the displaced footing area have not been removed for this analysis. Movements are relatively small compared with footing diameter, and therefore any error is negligible.

STRAIN CALCULATION

Strains can be calculated following Osman & Bolton (2005) by taking the first derivative of displacement. These are given by

$$\varepsilon_r = -\frac{\partial u}{\partial r} \quad \gamma_{r\theta} = 0 \tag{31a}$$

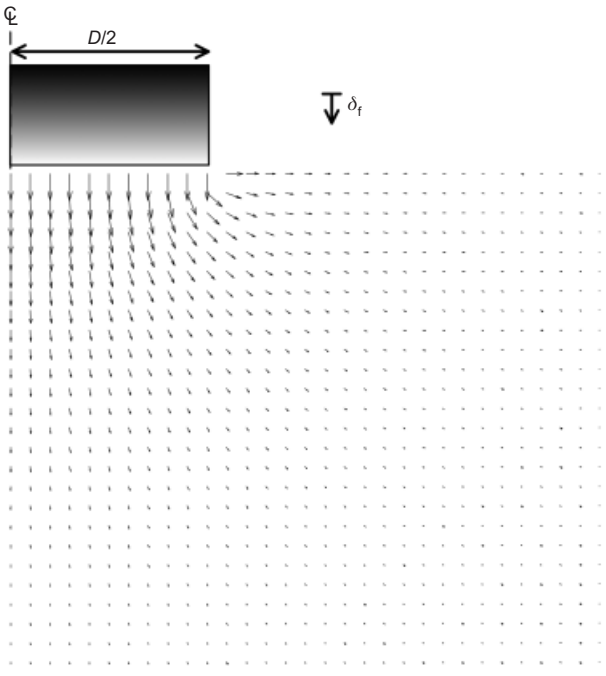

Fig. 4. Mechanism produced using the model

$$\varepsilon_\theta = -\frac{u}{r} \quad \gamma_{\theta z} = 0 \tag{31b}$$

$$\varepsilon_z = -\frac{\partial v}{\partial z} \quad \gamma_{rz} = -\frac{\partial v}{\partial r} - \frac{\partial u}{\partial z} \tag{31c}$$

The major and minor principal strains, ε_1 and ε_3, and the intermediate principal strain, ε_2 can be determined by

$$\varepsilon_1 = \tfrac{1}{2}\left(-\varepsilon_\theta + \sqrt{\varepsilon_\theta^2 + \gamma_{rz}^2 - 4\varepsilon_r\varepsilon_z}\right) \tag{32a}$$

$$\varepsilon_2 = \varepsilon_\theta \tag{32b}$$

$$\varepsilon_3 = \tfrac{1}{2}\left(-\varepsilon_\theta - \sqrt{\varepsilon_\theta^2 + \gamma_{rz}^2 - 4\varepsilon_r\varepsilon_z}\right) \tag{32c}$$

WORK CALCULATION

Elastic work beyond the bounding radius

Using the elastic solution of Yu (2000), and assuming no initial in situ stress

$$\sigma_c = \frac{4G\delta_b}{r_b} \tag{33}$$

Compatibility demands that $\delta_b = r_f^2\delta_f/2r_b^2$, and therefore the rate of elastic work outside the bounding radius can be shown to be

$$\frac{\partial W_b}{\partial \delta_f} = 2\pi G\frac{r_f^4}{r_b^3}\delta_f \tag{34}$$

Load–settlement behaviour

The rate of elastic work outside the boundary radius was added to the rates of plastic and elastic work, integrated over the appropriate regions within the bounding radius, and equated to the footing work. The relationship between footing stress and displacement is hence

$$\sigma_f = \frac{1}{\pi r_f^2}\left(\frac{\partial W_b}{\partial \delta_f} + \int_{\text{elastic}}\frac{\partial W_e}{\partial \delta_f}\mathrm{d}V + \int_{\text{plastic}}\frac{\partial W_p}{\partial \delta_f}\mathrm{d}V\right) \tag{35}$$

The process of solving equation (35) for all foundation settlements was computationally inexpensive, as the mechanism does not change with settlement. The work derivative terms are thus constant throughout the process. As the integration of the work terms is carried out numerically rather than analytically, the plastic radius need not be explicitly calculated. By comparing the strain invariant, $\hat{\varepsilon}$, with its value at yield given by equation (13), it can be determined whether any soil element is undergoing plastic or elastic deformation, and hence which expression of work is appropriate.

The preceding analysis has been formulated in terms of the triaxial compressive strength of the soil, q_u. In order to facilitate comparison with previously published finite-element analyses, it will be assumed that

$$q_u = 2c_u \tag{36}$$

RESULTS

Effect of hemispherical radius

The normalised footing pressure σ_f/c_u reduced as the ratio of hemispherical radius to footing diameter, r_h/D, increased. For a soil with $G/c_u = 100$ at a settlement of 5% of the footing diameter, the load–settlement behaviour is shown in Fig. 5. Beyond approximately two footing diameters there is minimal change in the calculated bearing stress with increas-

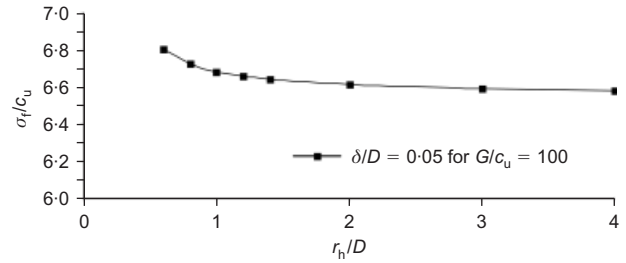

Fig. 5. Effect of increasing extent of ellipsoidal mechanism

ing hemispherical radius. Results for the load–settlement behaviour were therefore determined using a hemispherical radius of two footing diameters.

Effect of mesh size

A mesh size of 0·2%D was adopted for the analysis. A finer mesh, corresponding to a size 0·04%D, resulted in a reduction of the footing load by only 0·7%. The significant increase in computation time was therefore not justified.

Load–settlement behaviour

In order to make comparisons with previously published finite-element results, soils with values of rigidity, G/c_u, of 100 and 167 were considered. Figs 6 and 7 portray the load–settlement behaviour for these soils at varying values of settlement ratio. Fig. 6 also shows data from the finite-element analysis of Taiebat & Carter (2000, 2010) for a soil with $G/c_u = 100$, and Fig. 7 that of Gourvenec & Randolph (2002) for a soil with $G/c_u = 167$. The figures also show a line to represent the classical value of $N_c = 6{\cdot}05$ (Eason & Shield, 1960). Results agree well between the present study and the finite-element analyses, especially in the low-settlement region in which conventional design would be likely to take place. Analyses by Taiebat & Carter (2000, 2010) demonstrate approximately linear load–settlement behaviour in the small-settlement region. This is not reflected in the results of the present study, nor in those of Gourvenec & Randolph (2002), as the soil beneath the edge of the footing was observed to become plastic at very small settlements.

It is evident from Figs 6 and 7 that the footing pressure increases with the allowable footing settlement. Taiebat & Carter (2000) found that with a purely vertical load on the foundation no peak load was observed. Gourvenec & Randolph (2002) and Taiebat & Carter (2010), however, found convergence to limiting values of $N_c = 5{\cdot}91$ and 6·17 for soils with $G/c_u = 167$ and 100 respectively. While the load–settlement behaviour compares very well in the small settlement range, the results of this analysis continue to increase beyond the limiting value of $N_c = 6{\cdot}05$ at large settlements.

The analysis described in this paper gives an upper bound on foundation loading. Although it appears accurate when compared with the finite-element solutions at small settlements, it overestimates the strength of the foundation at large settlements. It is probable that once the footing settlement becomes large, the Prandtl mechanism will give a lower upper-bound on applied stress.

Implications for design

Analyses were performed on soils with G/c_u values between 10 and 10 000. The load–settlement behaviour was found to fall on a single line when plotted as a function of soil rigidity, G/c_u, multiplied by the normalised settlement, δ/D. Fig. 8 shows the relationship between the footing load and the soil rigidity multiplied by normalised settlement. The linear range of Fig. 8 represents the region of typical footing designs for clays. The expression for this range is

$$\frac{\sigma_f}{c_u} = 4{\cdot}45 + 1{\cdot}34 \ln\left(\frac{\delta}{D}\frac{G}{c_u}\right) \tag{37}$$

Equation (37) could be used in design in order to determine the allowable footing pressure based on an allowable settlement and the soil's rigidity.

As an example, consider a 2 m diameter footing with an allowable immediate undrained settlement of 2 mm founded on London Clay. Additional settlements due to consolidation would, of course, also need to be accounted for. It was suggested by Jefferies (1995) that a typical value of G/c_u for London Clay might be 180. Using these values in equation (37) produces $\sigma_f/c_u = 2{\cdot}15$, as indicated in Fig. 8. In conventional design terms this is equivalent to a factor of safety of 2·8 on the classical bearing capacity factor of 6·05. This single calculation has accounted for both bearing capacity and settlement.

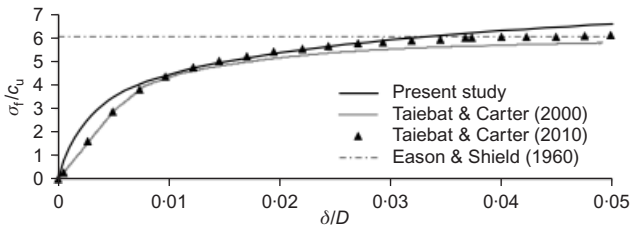

Fig. 6. Load–settlement behaviour for soil with $G/c_u = 100$

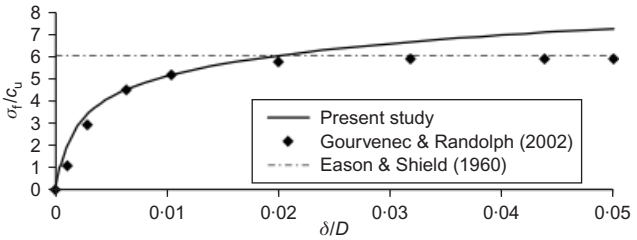

Fig. 7. Load–settlement response for soil with $G/c_u = 167$

CONCLUSIONS

An analysis to determine the load–settlement behaviour of a linear-elastic perfectly plastic soil by utilising cavity expansion methods has been presented. An upper-bound energy approach was adopted utilising an axisymmetric mechanism with displacements normal to ellipsoids, as shown in Fig. 4. The von Mises' yield criterion with

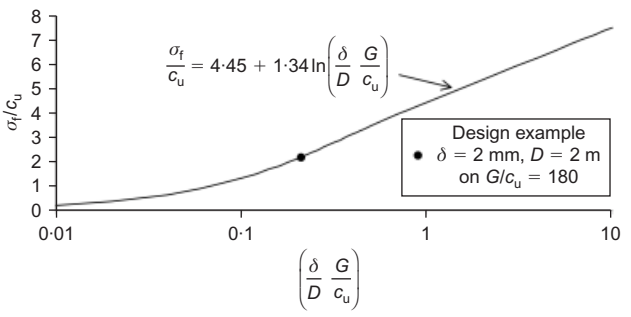

Fig. 8. Footing stress plotted against ($G/c_u \times \delta/D$) with expression for linear range and design example point

associated flow was utilised to determine the plastic work. The results were found to match very well in the small-settlement region with those produced from finite-element analyses.

A parametric investigation was performed, which demonstrated that when the footing load was plotted against the rigidity index multiplied by normalised settlement, a single line was produced, as shown in Fig. 8. The linear region of this plot represents the design region for shallow foundations, and is expressed as equation (37).

ACKNOWLEDGEMENTS

The first author would like to express his thanks for the financial support he received from the Cambridge Australia Trust (Poynton Scholarship) and the Principals of UK Universities (Overseas Research Students Awards Scheme) throughout his studies in Cambridge.

NOTATION

A_e	surface area of half ellipsoid
A_f	footing area
a	major-axis radius of ellipsoid
b	minor-axis radius of ellipsoid
c_u	undrained shear strength
D	footing diameter
E	elastic modulus
f	focal radius of ellipse
G	shear modulus
N_c	bearing capacity factor
p	mean principal stress
p_s	spherical cavity limit pressure
q_u	undrained strength in triaxial compression
q_{ult}	bearing capacity of footing
r	radial coordinate
r_b	boundary radius of analysis
r_c	radius of cavity
r_f	footing radius
r_h	hemispherical radius
r_p	plastic radius
s_c	shape factor
u	radial displacement
V	volume of cavity
$\mathrm{d}V$	change in cavity volume
v	vertical displacement
W	work
W_b	work outside analysis boundary
W_e	elastic work
W_f	footing work
W_p	plastic work
w	normal displacement
z	depth
$\gamma_{r\theta}$, $\gamma_{\theta z}$, γ_{rz}	shear strain in $r-\theta$, $\theta-z$ and $r-z$ planes respectively
δ_b	boundary settlement
δ_f	footing settlement
ε_1, ε_2, ε_3	major, intermediate and minor principal strains respectively
$\dot{\varepsilon}_1$, $\dot{\varepsilon}_2$, $\dot{\varepsilon}_3$	major, intermediate and minor principal strain rates
$\dot{\bar{\varepsilon}}$	a strain rate invariant
ε_r, ε_θ, ε_z	radial, circumferential and vertical strain
θ	angular coordinate
ν	Poisson's ratio
ρ	cavity radial displacement
σ_b	boundary stress
σ_f	footing pressure
σ_1, σ_2, σ_3	major, intermediate and minor principal stresses
$\hat{\sigma}_1$, $\hat{\sigma}_2$, $\hat{\sigma}_3$	major, intermediate and minor deviatoric stresses

REFERENCES

Bishop, R. F, Hill, R. & Mott, N. F. (1945). The theory of indentation and hardness tests. *Proc. Phys. Soc.* **57***, Part 3, 147–159.*

Cox, A. D, Eason, G. & Hopkins, H. G. (1961). Axially symmetric plastic deformations in soils. *Phil. Trans. R. Soc. London (Ser. A)* **254**, No. 1036, 1–45.

Eason, G. & Shield, R. T. (1960). The plastic indentation of a semi-infinite solid by a perfectly rough circular punch. *Z. Angew. Math. Phys*. **11**, No. 1, 33–43.

Gourvenec, S. & Randolph, M. (2002). Effect of strength non-homogeneity on the bearing capacity of circular skirted foundations subjected to combined loading. *Proc. 11th Int. Offshore Polar Engng Conf., Kyushu*, 693–698.

Jefferies, M. G. (1995). Discussion on 'The effects of pressuremeter geometry on the results of tests in clay', by G. T. Houlsby and J. P. Carter. *Géotechnique* **45**, No. 4, 741–744, http://dx.doi.org/10.1680/geot.1995.45.4.741.

Klar, A. & Osman, A. S. (2008). Load–displacement solutions for piles and shallow foundations based on deformation fields and energy conservation. *Géotechnique* **58**, No. 7, 581–589, http://dx.doi.org/10.1680/geot.2007.00128.

Martin, C. M. (2003). New software for rigorous bearing capacity calculations. *Proceedings of the international conference on foundations*, Dundee, pp. 581–592.

McMahon, B. T. (2012). *Deformation mechanisms below shallow foundations*. PhD thesis, Univeristy of Cambridge, UK.

Osman, A. S. & Bolton, M. D. (2005). Simple plasticity-based prediction of the undrained settlement of shallow circular foundations on clay. *Géotechnique* **55**, No. 6, 435–447, http://dx.doi.org/10.1680/geot.2005.55.6.435.

Prandtl, L. (1921). Über die Eindringungsfestigkeit plastischer Baustoffe und die Festigkeit von Schneiden. *Z. Ange. Math. Mech*. **1**, No. 1, 15–20.

Shield, R. T. & Drucker, D. C. (1953). The application of limit analysis to punch-indentation problems. *J. Appl. Mech*. **20**, No. 4, 453–460.

Taiebat, H. A. & Carter, J. P. (2000). Numerical studies of the bearing capacity of shallow foundations on cohesive soil subjected to combined loading, *Géotechnique* **50**, No. 4, 409–418, http://dx.doi.org/10.1680/geot.2000.50.4.409.

Taiebat, H. A. & Carter, J. P. (2010). A failure surface for circular footings on cohesive soils. *Géotechnique* **60**, No. 4, 265–273, http://dx.doi.org/10.1680/geot.7.00062.

Terzaghi, K. (1943). *Theoretical soil mechanics*. New York, NY, USA: John Wiley & Sons.

White, D. J., Take, W. A. & Bolton, M. D. (2003). Soil deformation measurement using particle image velocimetry (PIV) and photogrammetry. *Géotechnique* **53**, No. 7, 619–631, http://dx.doi.org/10.1680/geot.2003.53.7.619.

Yu, H. S. (2000). *Cavity expansion methods in geomechanics*. Dordrecht, the Netherlands: Kluwer Academic.